Journal of the Brazilian Society of Mechanical Sciences and Engineering (2021) 43:231
https://doi.org/10.1007/s40430-021-02946-1

TECHNICAL PAPER

Inclination angle effect of tribological performance for hydrostatic bearing having tilting oil pad under variable viscosity conditions

Xiaodong Yu[1] · Guangpeng Wu[1] · Wenkai Zhou[1] · Hongwei Bi[1] · Yu Wang[1] · Weicheng Gao[1] · Junfeng Wang[2] · Jianhua Jiao[2] · Hui Jiang[2]

Received: 30 August 2020 / Accepted: 15 March 2021 / Published online: 1 April 2021

Abstract
In order to improve tribological performance of hydrostatic bearing, an innovative hydrostatic bearing structure having tilting oil pad is designed. During the operation, the semicircular boss at the bottom of the oil pad can realize the circumferential micro-motion. It generates additional dynamic pressure, and forms the static and dynamic pressure mixing support, make up for the static pressure loss, and solves the problems such as low precision and unstable operation of the numerical control equipment under the high speed and heavy load conditions. According to the tribological principle and lubrication theory, bearing capacity, flow rate, oil film thickness equation and oil film stiffness for hydrostatic and dynamic hybrid bearing are derived under variable viscosity conditions. The simulation model of hydrostatic bearing having tilting oil pad is established. ANSYS software is used to analyze the distribution of oil film temperature field and oil film pressure field under different inclination angles. The effects of tilting oil pad inclination angle on oil film tribological performance and oil film stiffness are obtained. The results show that the hydrostatic bearing having tilting oil pad can generate additional dynamic pressure in high speed operation, make up the loss of static pressure. When the inclination angle is 0.0044°, oil film temperature rise is 34.8 ℃, the average pressure is 622.2 KPa, oil film stiffness is 54104 N/μm, the comprehensive lubrication performance is optimal, the oil film stiffness is the largest, and the operation accuracy and stability of hydrostatic bearing are improved.

Keywords Oil pad inclination angle effect · Hydrostatic and dynamic hybrid bearing · Oil film stiffness · Tribological performance · Theoretical analysis and experimental research

1 Introduction

For the hydrostatic bearing worktable running under the condition of high speed and heavy load, the extrusion heating and shear heating will be very large, the viscosity of the lubricating oil will decrease more, the oil film distribution will be uneven and thinner, the stiffness will decrease, and the local boundary lubrication or even dry friction will occur, which leads to tribological failure. Researchers at home and abroad seek a variety of ways and means to solve such problems.

Chen et al. [1] put forward the elliptical flexible hinge tilting pad bearing. Based on the stiffness modeling of the flexure hinge, the influence of the rotational stiffness of the flexure hinge on the dynamic and static performance of the bearing is studied by using the finite difference method and Newton iterative method. Taking into account, the temperature viscosity effect of lubricating oil and the differential equation of journal-tile motion, Yang et al. [2] establish its dynamic model based on flexible support tilting pad bearing, and it compares the relevant literature test data. Liu and Chen [3, 4] prepared a tilting pad bearing with fulcrum elasticity and damping characteristics, which can increase the critical damping of the rotor and effectively improve the stability of the rotor system. Yu et al. [5] established the thermal elasto-hydrodynamic lubrication mathematical model of tilting

Technical Editor: Daniel Onofre de Almeida Cruz.

✉ Xiaodong Yu
yuxiaodong@hrbust.edu.cn

[1] Key Laboratory of Advanced Manufacturing and Intelligent Technology, Ministry of Education, Harbin University of Science and Technology, Heilongjiang Province, Harbin 150080, China

[2] Qiqihar Heavy CNC Equipment Corp. LTD, Qiqihar 161005, China

pad bearing under transient condition and studied the transient lubrication performance at start. Finally, the bearing axis trajectory, oil film thickness, fluid dynamic pressure, tile surface temperature, and tile surface thermoelastic deformation from the initial position to the equilibrium position are obtained. Zhang et al. [6] used ANSYS to simulate the effects of inlet oil pressure, inlet oil temperature, eccentricity, and journal speed on the oil film characteristics of four-watt tilting pad bearings. Zhu et al. [7] studied the tile swing characteristics of fan guide bearings supported by four tilting pads and found that the tile swing angle characteristics are determined by the circumferential relative position of the tile and the load, preload, and eccentricity. Zhang et al. [8] used Fluent software to simulate the flow field of the traditional four-pad hydrostatic support and the new asymmetric hydrostatic support structure. The simulation results show that the friction of the new asymmetric hydrostatic support structure is small, and the piston rod can be adaptively balanced when the piston rod is subjected to radial offset. In order to improve the safety and reliability of traditional rigid fulcrum tilting pad radial bearing, Jin et al. [9] put forward a kind of elastic fulcrum tilting pad radial bearing for vertical rotor, which is an adjustable fulcrum and can realize adaptive pretension. Yang et al. [10] studied the effect of high temperature imported oil on the comprehensive performance of tilting pad bearings and carried out experiments. The oil film thickness, bearing temperature rise, and vibration amplitude at different inlet oil temperatures are obtained. Okabe [11] uses the short bearing method to establish the model of tilting pad bearings and takes into account the effects of turbulence and fluid inertia under high speed conditions. Suh and Choi [12] studied the angular deviation between tilting pad radial sliding bearing and rotating journal, and put forward a three-dimensional numerical model considering bearing tilt, pitching and yaw motion, journal deformation, journal angular motion and thermo-hydrodynamic lubrication model. Li et al. [13] uses the finite difference method to solve the equations for controlling flow and energy transfer, and makes a theoretical study on the temperature of the high-speed and heavy-load tilting pad radial sliding bearing. The experimental study is carried out on the high-speed and heavy-load tilting pad radial sliding bearing test-bed. Wang et al. [14–17] gave a numerical solution method for the lubrication characteristics of the sliding pair considering the dynamic pressure effect and simulated its lubrication characteristics. The results showed that the center oil film thickness and the maximum inclination angle of the sliding shoe are the main influencing factors of the oil film dynamic pressure effect.

A new type of oil pad tilting hydrostatic bearing is proposed, which automatically realizes small angle circumferential tilt during operation, provides the conditions for the generation of dynamic pressure, generates additional dynamic pressure, and turns the hydrostatic bearing into a hydrostatic hybrid thrust bearing. Its comprehensive lubrication performance and oil film stiffness are higher than those of hydrostatic bearings, which can be used to solve the problems of low machining accuracy and poor stability of vertical CNC equipment under the condition of high speed and heavy load.

2 Structure and principle of oil pad tilting static and dynamic bearing

The oil pad tilting type static and dynamic pressure bearing is composed of a rotating worktable, a base, and a differentiable pendulum oil pad. 12 static and dynamic oil pads are evenly distributed on the guide rail, which are separated by oil return grooves, and the oil pad tilting type static and dynamic pressure bearing structure is shown in Fig. 1.

A semicircular convex platform is arranged under the oil pad, which can swing at any small angle in the circumferential direction to form an inclinable oil pad, which meets the conditions for the formation of dynamic pressure, and it realizes the mixed lubrication of static and dynamic pressure [18–23]. The static and dynamic pressure mixed support structure is shown in Fig. 2, and the working principle is shown in Fig. 3.

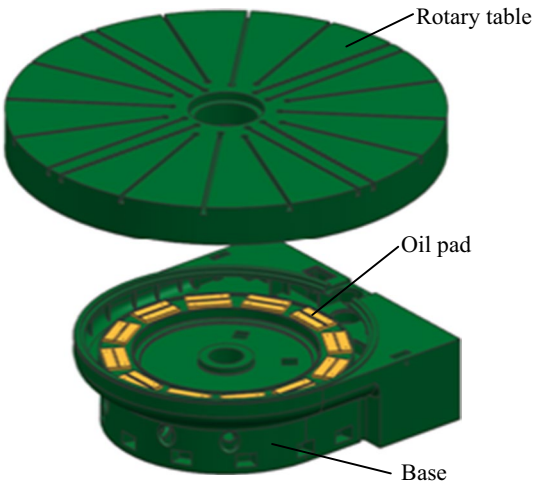

Fig. 1 Static and dynamic pressure mixed lubrication support structure

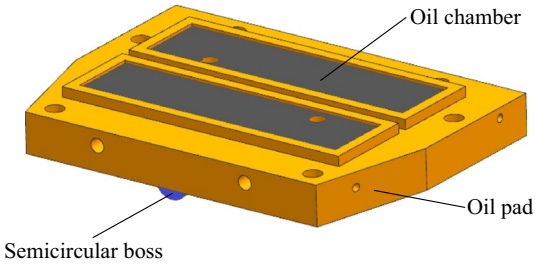

Fig. 2 Tilting oil pad

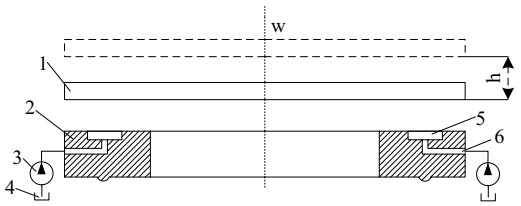

1-Rotate the worktable 2-Hydrostatic guideway 3-Quantitative fuel supply pump 4-Fuel tank 5-Tilting oil cavity 6-Intake pipe W-External load h-Pressure oil film

Fig. 3 Static/dynamic pressure support working principle diagram. (1) Rotate the worktable, (2) hydrostatic guideway, (3) quantitative fuel supply pump, (4)fuel tank, (5) tilting oil cavity, (6) intake pipe W-external load *h*-pressure oil film

3 Tribological energy control equation of static and dynamic bearing

3.1 Viscosity–temperature relationship of lubricating oil

According to the 32# lubricating oil viscosity temperature relationship table, as shown in Table 1, the software fitting the 32# lubricating oil viscosity temperature relationship curve is shown in Fig. 4.

According to Fig. 4, the viscosity and temperature of # 32 lubricating oil are exponentially distributed, and the exponential function relationship is obtained.

$$y = a \times e^{-\left(\frac{x-b}{c}\right)^2} \tag{1}$$

where $a = 4.47 \times 1028$, $b = -2048$, $c = 250.2$.

Therefore, the viscosity–temperature relationship equation is:

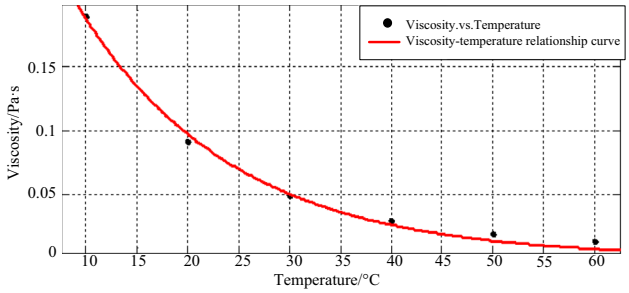

Fig. 4 32# Lubricant viscosity–temperature curve

$$\mu = 4.47 \times 10^{28} e^{-\left(\frac{T_0+\Delta T+2048}{250.2}\right)^2} \tag{2}$$

where T_0 is the inlet temperature (℃) and ΔT is the outlet temperature rise (℃).

3.2 Bearing capacity equation

Since the double rectangular oil cavity is a combination of two identical rectangular cavities, a rectangular cavity is used for calculation, and its pressure is approximately uniformly distributed as shown in Fig. 5, and the structure and effective area of the rectangular cavity are shown in Fig. 6. Then, the bearing capacity of a single rectangular cavity is:

$$\begin{aligned} w &= p(B-2b_1)(L-2l_1) \\ &\quad + \frac{p}{2}[LB-(B-2b_1)(L-2l_1)] \\ &= p[(L-l)(B-b_1)+l_1b_1 \\ &= pLB\left[\left(1-\frac{l_1}{L}\right)\left(1-\frac{b_1}{B}\right)+\frac{l_1}{L}+\frac{b_1}{B}\right] \end{aligned} \tag{3}$$

where $l_1 = \frac{L-l}{2}$, $Q = \frac{bh^3\Delta p}{12\mu l}$, if the influence of $\frac{l_1 b_1}{LB}$ is ignored, the above equation can be simplified to:

$$W_s = pLB\left(1-\frac{l}{L}\right)\left(1-\frac{b}{B}\right) = p(L-l_1)(B-b_1) = pA_e \tag{4}$$

The bearing capacity of the double rectangular oil chamber is obtained as follows:

$$W_d = 2pA_e \tag{5}$$

where A_e is the effective bearing area of the oil cavity.

Table 1 32# Lubricating oil viscosity parameter table

Temperature (℃)	10	20	30	40	50	60
Kelvin temperature (K)	283	293	303	313	323	333
Viscosity (Pa·s)	0.1900	0.0907	0.0487	0.0288	0.0184	0.0125

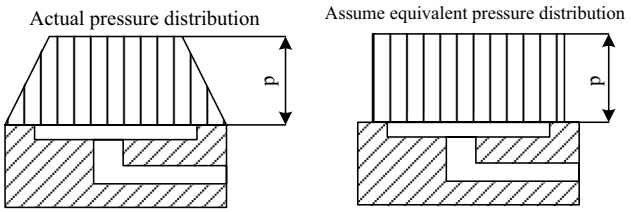

Fig. 5 Oil pressure distribution from single rectangular chamber

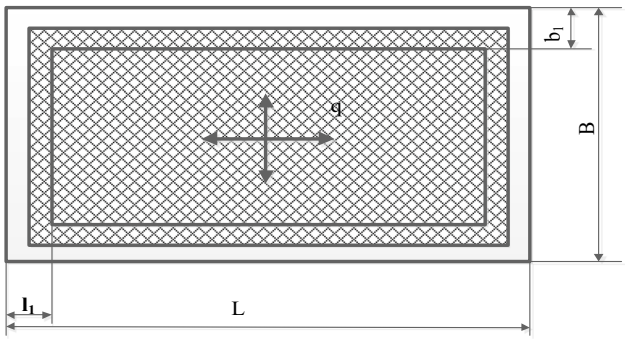

Fig. 6 Single rectangular cavity structure and effective area

3.3 Flow equation

The clearance between the rotating table and the base of the hydrostatic bearing is a parallel plate, so the flow equation can be deduced and calculated according to the gap flow formula between the parallel plates.

When the film thickness is h, the flow rate Q through the oil pad can be calculated in the two flow directions of X and Y, respectively:

$$Q_X = 2\frac{h^3(B-b)\Delta p}{12\mu l} \tag{6}$$

$$Q_Y = 2\frac{h^3(L-l)\Delta p}{12\mu b} \tag{7}$$

The total flow caused by the combined action of differential pressure and shear force is the sum of X-direction and Y-direction flow.

The flow through the rectangular cavity is:

$$Q = \frac{\Delta p h^3}{6\mu}\left[\frac{B-b_1}{l_1} + \frac{L-l_1}{b_1}\right] \tag{8}$$

where Δp is the pressure difference and μ is the dynamic viscosity.

The flow through a double rectangular cavity:

$$Q_d = \frac{\Delta p h^3}{3\mu}\left[\frac{B-b_1}{l_1} + \frac{L-l_1}{b_1}\right] \tag{9}$$

3.4 Oil film thickness equation

Figure 7 shows that the oil film of static and dynamic pressure mixed support of tilting oil pad is composed of central support oil film, circumferential inclined oil film, and elastic deformation, and the shape of oil film is shown in Fig. 7.

Central support oil film thickness:

$$h_z = h_0 \tag{10}$$

Circumferential inclined oil film thickness:

$$h_\theta = M_\theta \cdot \left[r \cdot \sin\left(\theta - \frac{\theta_r}{2}\right)\right] \tag{11}$$

Elastic deformation thickness:

$$h_\delta = \delta_{\max}\frac{r^2 + R_0^2 - 2rR_0 \cdot \cos\left(\theta - \frac{\theta_r}{2}\right)}{R_2^2 + R_0^2 - 2R_2R_0 \cdot \cos\frac{\theta_r}{2}} \tag{12}$$

Total oil film thickness:

$$h = h_z + h_\theta + h_\delta \tag{13}$$

Further arrangement is available:

$$h = h_0 = M_\theta \cdot \left[r \cdot \sin\left(\theta - \frac{\theta_r}{2}\right)\right] + h_\delta \tag{14}$$

where θ and γ are polar coordinate elements; h_0 is the film thickness at the central support; $\delta_{\max}$ is the maximum deformation deflection; R_0 is the distance from the center of the tilting oil pad to the axis of rotation; R_2 is the maximum radius of deformation; M_θ is the circumferential tilt angle.

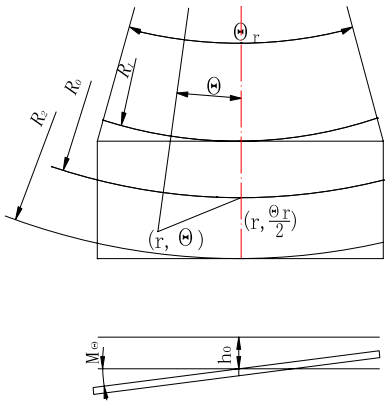

Fig. 7 Oil film shape

3.5 Oil film stiffness

The differential of bearing capacity to the thickness of oil film is the stiffness of oil film.

$$J = \frac{dW}{dh} = \frac{3P_s \cdot A_e \cdot p_0}{h} \tag{15}$$

where P_s is the input pressure of the oil supply system; A_e is the effective bearing area; P_0 is the ratio of the oil cavity pressure to the limited pressure in the design state; h is the oil film thickness.

4 Numerical simulation of tribological properties

4.1 Grid division

According to the actual production, the 20 t–140 r/min working condition is studied. The three-dimensional model of oil film is established by UG, and the thickness of oil film is 0.069 mm, as shown in Fig. 8. The three-dimensional model is imported into ANSYSICEM to divide the structured grid, and O-BLOCK is used to improve the grid quality of the oil hole [24, 25]. The total number of grids is 330,056, of which 0.9 ~ 1 grid accounts for 95.235% of the total grid, the angle standard is above 45°, the grid quality is very good. Figure 9 is the overall grid diagram of the oil film, and Fig. 10 is the schematic diagram of the quality of the oil film grid.

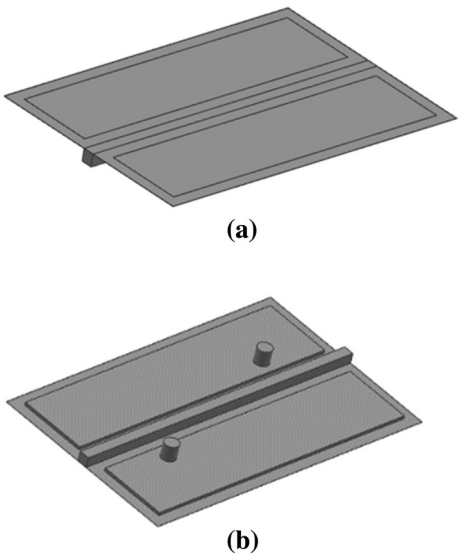

Fig. 8 Oil film three-dimensional model diagram

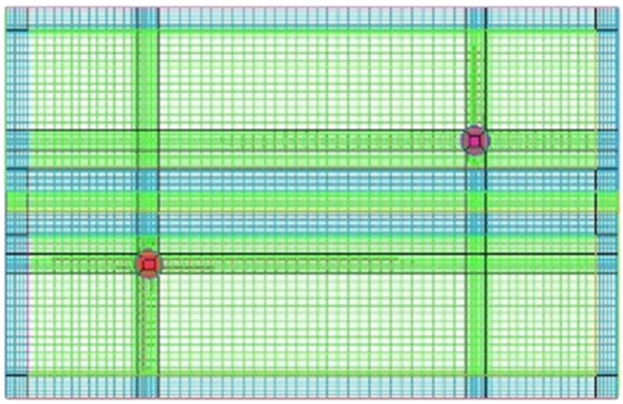

Fig. 9 Oil film overall grid diagram

4.2 Boundary condition

The boundary conditions are set in ICEM, the two entrances are set to IN1 and IN2, the four outlets are set to OUT1, OUT2, OUT3, and OUT4, the upper surface of the oil film is set to ROTA TE, both sides of the oil film are set as periodic boundary conditions INTERFACE1, and the rest of INTERFACE2 are set to WALL, as shown in Fig. 11.

4.3 Lubricating oil attribute setting

The viscosity–temperature relationship is set according to Eq. (15). The quantitative oil supply is adopted, the flow rate of the two oil inlets is 0.035 kg/s, the temperature is 293 K at room temperature, and the pressure at the outlet is atmospheric pressure.

5 Numerical simulation results and analysis

According to the engineering practice and related literature, the circumferential dip angle is selected from 0.0012° to 0.0060° [26]. And the maximum and minimum oil film

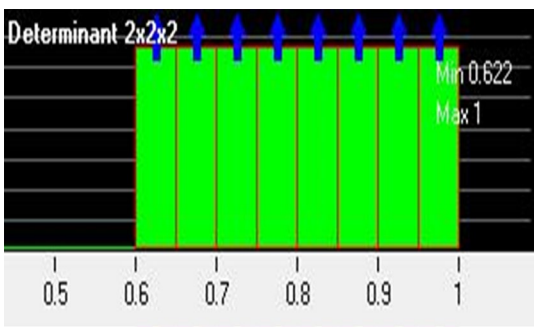

Fig. 10 Oil film grid quality diagram

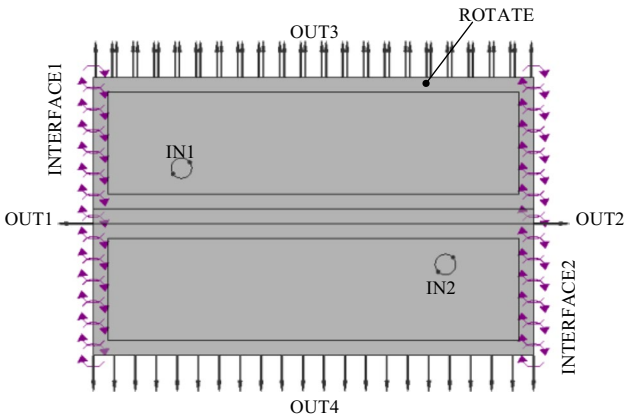

Fig. 11 Oil film boundary condition setting

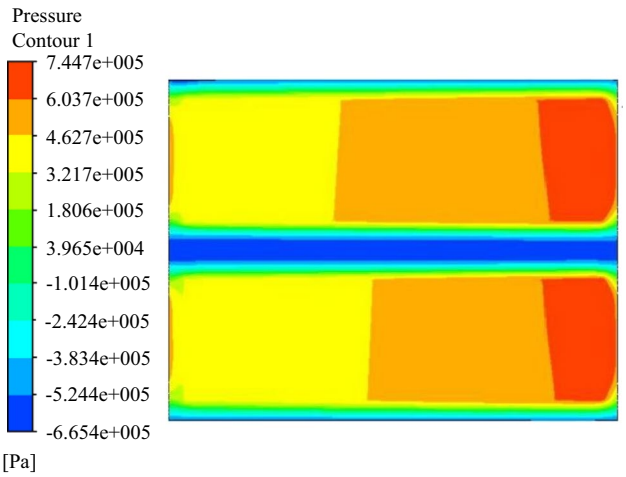

Fig. 12 Pressure field at an inclination angle of 0.0044°

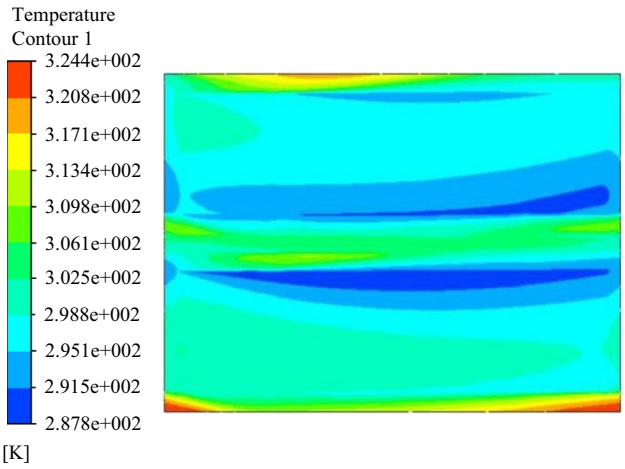

Fig. 13 Temperature field at an inclination angle of 0.0044°

thickness corresponding to the inclination angle from 0.0012° to 0.0060° calculated by formula (14) are shown in Table 2.

5.1 Effect of inclination angle on tribological properties

Under the condition of load 20 t and rotational speed 140 r/min, the static and dynamic oil film pressure and temperature under seven simulated dip angles ranging from 0.0012° to 0.0060° are limited by space, and only the pressure field and temperature field are given when the inclination angle is 0.0044°. As shown in Figs. 12 and 13, the relationship between pressure and inclination angle is shown in Fig. 14, and the relationship between oil film temperature and inclination angle is shown in Fig. 15.

It can be found from Figs. 12 and 14 that the circumferential pressure of the oil film increases along the rotation direction of the worktable under the working condition of 20 t load and 140 r/min speed, which is caused by the additional dynamic pressure when the lubricating oil flows from the oil cavity to the sealing edge. The maximum pressure increases at first and then decreases with the increase in inclination angle, and the maximum value appears when the inclination angle is 0.0044°, and the bearing effect of oil film is the best.

It can be seen from Figs. 13 and 15 that the temperature field distribution of the oil film is uneven and the local high temperature occurs because the oil film is subjected to the combined action of extrusion pressure and transverse shear force. When the oil film rotates, due to the influence of shear, the outside heat is large, and the highest temperature appears on the outside of the sealing edge.

5.2 Effect of inclination angle on stiffness

Similar to the research process of load 20 t and speed 140 r/min, use CFX to post-process the software simulation results, select the "ave and force" options in FUNCTION Calculator to get the average pressure and oil film stiffness of the oil chamber under different inclination angles, as shown in Table 3.

Table 2 Maximum and minimum oil film thickness at different inclination angles

Inclination angle (°)	0.0012	0.0020	0.0028	0.0036	0.0044	0.0052	0.0060
h_{max} (mm)	0.0710	0.0723	0.0736	0.0750	0.0763	0.0776	0.0789
h_{min} (mm)	0.0670	0.0657	0.0644	0.0630	0.0617	0.0604	0.0591

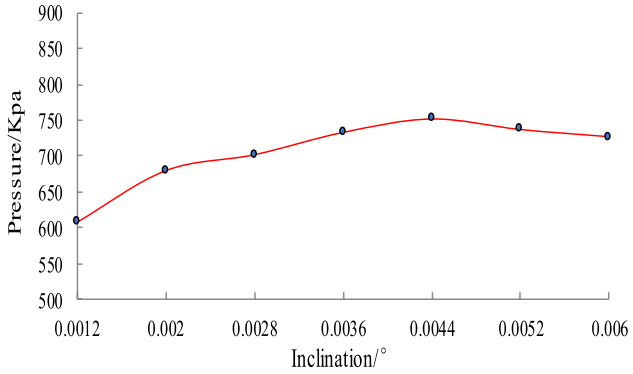

Fig. 14 Oil film pressure and inclination angle

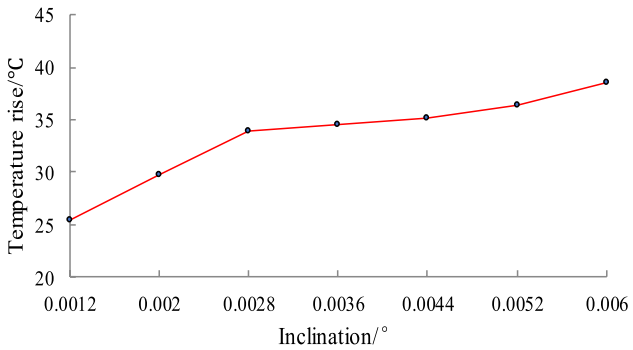

Fig. 15 Oil film temperature and inclination angle

It can be seen from Table 3 that the average pressure of the oil cavity and the oil film stiffness first increases and then decreases with the increase in the inclination angle. When the inclination angle is 0.0044°, the oil cavity average pressure and oil film stiffness reach the maximum, and the oil film bearing capacity and stability are the best. With the increase in the inclination angle, the additional dynamic pressure formed by the movement of the oil film increases, which increases the bearing capacity and stiffness of the oil film. But when the inclination angle exceeds 0.0044°, the oil film there is too thin, which will cause the pressure and stiffness of the oil film to decrease.

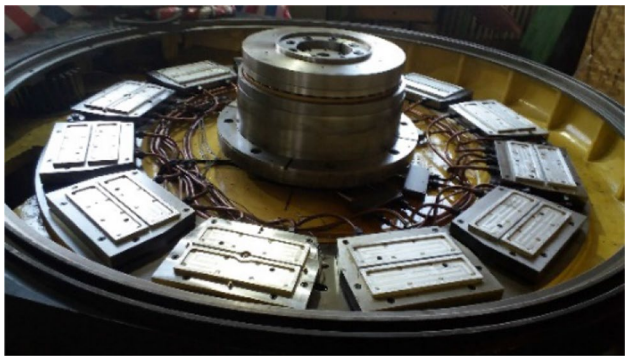

Fig. 16 Oil pad tilting static pressure bearing

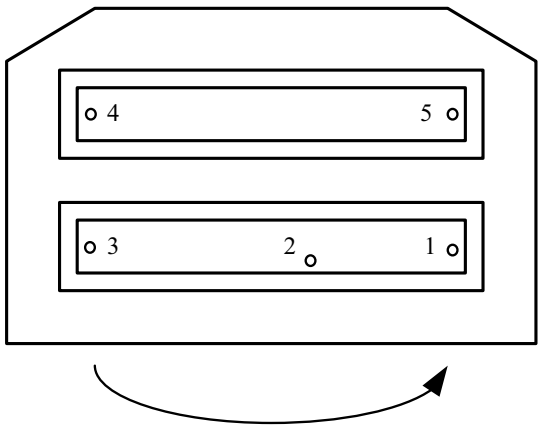

Fig. 17 Pressure sensor layout

6 Experimental study on tribological properties

In order to verify the correctness of theoretical analysis and numerical simulation, experiments were carried out on a certain type of vertical lathe worktable in a factory. The maximum cutting diameter of the machine tool is 3150 mm, the diameter of the worktable is 2830 mm, there are 12 double rectangular oil cavities, quantitative oil supply, maximum load capacity 40 t, maximum speed 200 r/min. The experimental device is shown in Fig. 16, the pressure sensor, temperature sensor, displacement sensor and pressure gauge are installed as shown in Figs. 17, 18, 19 and 20, and the data acquisition and display system are shown in Fig. 21. The pressure sensor is a piezoresistive pressure transmitter with a working voltage of 24 VDC, a measuring range of

Table 3 Oil film pressure and stiffness vary with inclination angle

Inclination angle (°)	0.0012	0.0020	0.0028	0.0036	0.0044	0.0052	0.0060
Average pressure (KPa)	590.2	591.8	594.8	600.7	622.2	596.1	593.1
Greatest pressure (KPa)	609.2	686.3	701.5	712.7	744.7	716.8	715.7
Stiffness (N/μm)	51,322	51,461	51,722	52,235	54,104	51,835	51,574

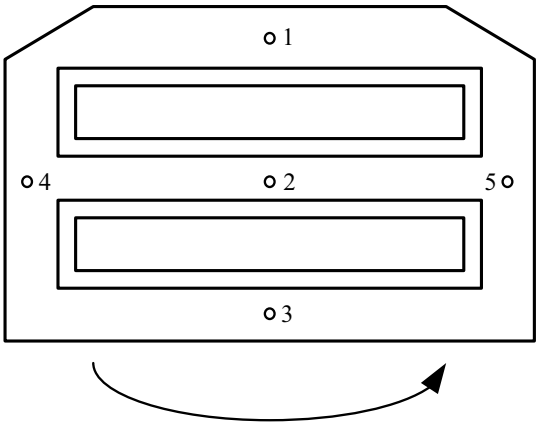

Fig. 18 Temperature sensor layout

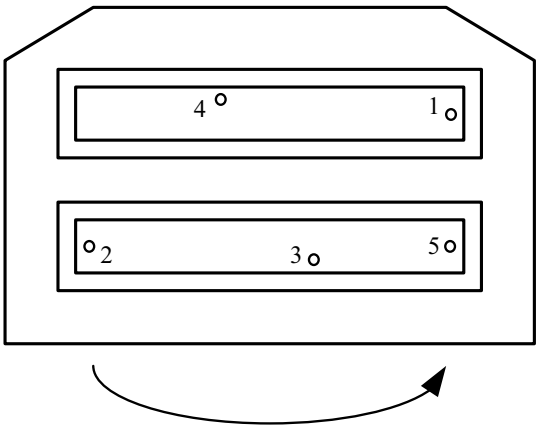

Fig. 19 Displacement sensor layout

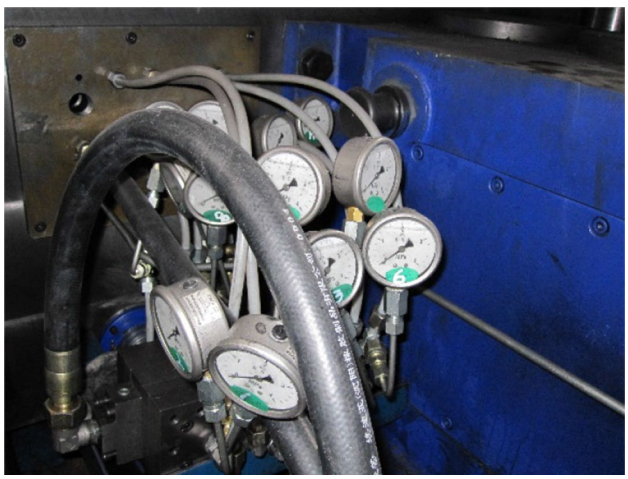

Fig. 20 Pressure gauge layout

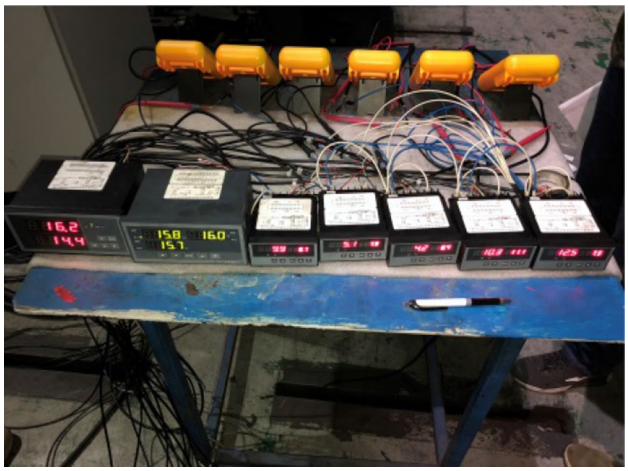

Fig. 21 Data acquisition and display system

−0.1 to 100 MPA and an accuracy of ± 0.25%FS. The average pressure of the oil cavity is measured by the pressure gauge, the temperature sensor is an integrated temperature transmitter, the measuring range is −200 ℃ ~ 1600 ℃, and the measuring accuracy can reach 0.5%. The working voltage of the displacement inductance sensor is 24VDC, the measuring range is 0.25 and 1.25 mm, and the highest sensitivity is more than 0.1 μm. Since each adjustment of the oil pad inclination angle requires the lifting of the rotating table and the fixed workpiece, the reinstallation process is extremely difficult, and the result may be affected by the eccentric load caused by the placement of the workpiece. This experiment is mainly to verify the correctness of the simulation method. So limited by the field conditions, the pressure field, temperature field, average pressure, and oil film stiffness are only verified when the inclination angle is 0.0044°. Adjust the height of the bolt at the bottom of the oil pad so that there is a fixed height difference between the two bolts, and the adjusted inclination angle can be calculated by the distance. The displacement sensor is used to verify the displacement of the oil pad bolt position, ensuring that the inclination is 0.0044°.

6.1 Experimental method

When the ambient temperature is 15 ℃ and the worktable is loaded with 20 t, the oil film temperature, oil film pressure, and oil film thickness are measured at different rotational speeds.

6.2 Experimental results and data analysis

The experiment adopts the method of measuring the average value for many times, and the pressure and temperature of

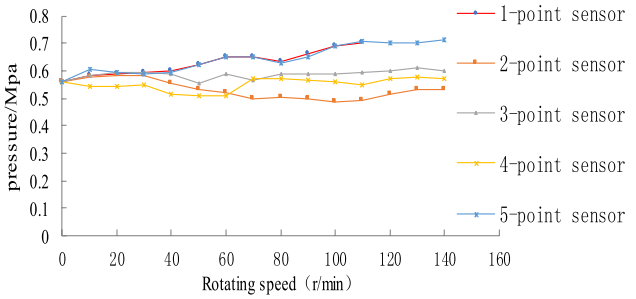

Fig. 22 Pressure at different oil chamber positions varies with speed

different oil cavity positions vary with the rotational speed, as shown in Figs. 22 and 23.

It can be seen from the above Fig. 22 that when the load is 20 t, the pressure at 3 and 5 points increases gradually, which is caused by the dynamic pressure, and the pressure at the other three points gradually decreases, which is consistent with the distribution law of the pressure field in Fig. 12.

As can be seen from the Fig. 23 above, with the increase in rotating speed, the temperature rises rapidly and changes significantly, and the temperature rises at point 3 and point 5 are the highest. Point 3 is located outside the oil cavity, with large linear velocity and high shear clarification, point 5 is located at the downstream side of the oil cavity, forming dynamic pressure; point 3 and point 5 have large temperature rise, which is consistent with the temperature field distribution in Fig. 13. The average pressure of the oil cavity at 100–140 r/min is measured by the pressure gauge, and the average stiffness of the oil film is calculated, as shown in Table 4.

From the comparison between Tables 3 and 4, it can be found that the experimental values of average pressure and stiffness are in good agreement with the simulated values, and the error is 5%.

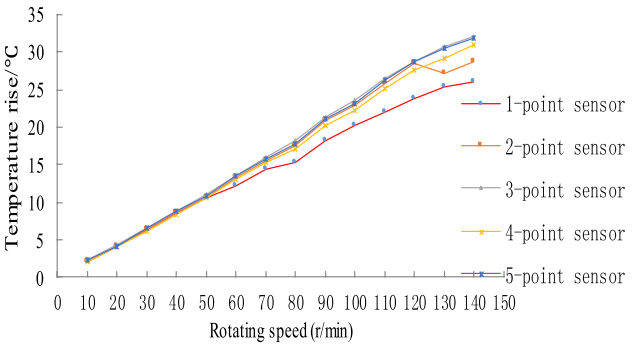

Fig. 23 Temperature rise of different oil chambers varies with speed

Table 4 Average pressure and average stiffness at different speeds

Rotating speed (r/min)	100	110	120	130	140
Average pressure (KPa)	604	608	620	623	626
Average stiffness (N/μm)	52,522	52,870	53,913	54,174	54,435

7 Conclusions

A novel hydrostatic bearing structure with tilting oil pad is proposed. The hydrostatic bearing structure can generate additional dynamic pressure in the process of operation, and can be converted into static and dynamic mixed hydrostatic bearing, and can solve the problems of machining accuracy and running stability of CNC equipment under high speed and heavy load conditions.

The bearing capacity equation, flow equation, film thickness equation, and oil film stiffness equation of tilting oil pad hydrostatic bearing with double rectangular cavity are derived, and the tribological performance of hydrostatic bearing is analyzed under the condition of variable viscosity. It is concluded that the tilting oil pad can produce additional dynamic pressure under the condition of high speed, and the influence of tilting angle on the tribological performance and oil film stiffness of the new tilting oil pad is revealed.

Through the simulation calculation of the inclination angle of the oil pad, the average pressure of the oil cavity and the oil film stiffness at different inclination angles under the same oil cavity area are obtained, and seven groups of data are comprehensively analyzed. The results showed that when the inclination angle is 0.0044°, the tribological performance, the average pressure and stiffness of the oil film are the highest, the bearing capacity is the largest, and the operation of the oil film is the most stable, which is verified by experiments. The tilting oil pad will generate additional dynamic pressure, thereby increasing the average pressure and stiffness of the oil film, and improving the stability and accuracy of the hydrostatic bearing.

In actual production, adjusting the nut under the oil pad can change the inclination angle of the oil pad and fix it, which can achieve higher processing quality under high speed and heavy load conditions.

Acknowledgment This research was financially supported by the National Natural Science Foundation of China (51375123) and the Natural Science Foundation of Heilongjiang Province (E2016040).

Compliance with ethical standards

Conflict of interest The authors declared no potential conflicts of interest with respect to the research, authorship, and publication of this article.

References

1. Chen S, Xiong W, Lu C et al (2018) Research on static and dynamic characteristics of flexure-pivot tilting pad journal bearings. J Vib Shock 37(2):236–241
2. Yang Y, Li W, Zhao X et al (2017) Full Dynamics modeling and analysis of flexure pivot tilting pad bearings. Noise Vib Control 37(6):7–11
3. Liu S, Xiao Z, Yan Z et al (2014) Numerical and experimental research on dynamic characteristics of tilting-pad journal bearing of pivot stiffness and damping. J Mech Eng 50(19):88–96
4. Chen Z, Liu S, Zheng T (2014) Experimental analysis on characteristics of the rotor system supported by tilting-pad journal bearing considering pivot stiffness and damping. J Fudan Univ (Nat Sci) 53(5):659–665
5. Yu J, Wang J, Wang Q (2014) Transient thermal EHD performance of multi-tilting-pad journal bearing. Lubr Eng 39(01):5–8
6. Zhang A, Li G, Dang C (2014) Effect of operating conditions on oil film properties of steam turbine tilting pad bearings. Lubr Eng 39(02):84-88+107
7. Zhu A, Yang Y, Chen W et al (2014) Swing characteristic of pads in four-pad tilting pad bearing. J Mech Eng 50(9):43–47
8. Zhang W, Li Ma, Zhao X et al (2019) Comparative simulation analysis of asymmetric hydrostatic support structure of servo hydraulic cylinder. Mach Tool Hydraul 047(015):145–151, 160
9. Jin Y, Chen F, Zhang F et al (2019) Nonlinear dynamic performance of tilting-pad journal bearing with adjustable elastic pivot design. Tribol Int 136
10. Yang P, Yuan Q, Chen R (2018) Experimental research on the tilting pad bearing under the high temperature of inlet oil. Ind Lubr Tribol 70(6)
11. Okabe EP (2017) Analytical model of a tilting pad bearing including turbulence and fluid inertia effects. Tribol Int 114
12. Suh J, Choi Y-S (2016) Pivot design and angular misalignment effects on tilting pad journal bearing characteristics: four pads for load on pad configuration. Tribol Int 102
13. Li P, Zhu Y, Zhang Y et al (2015) The investigation of the temperature of high speed and heavy haul tilting pad journal bearing. Ind Lubr Tribol 67(4)
14. Wang Y, Chen X, Cao H et al (2020) Simulation analysis of lubrication characteristics of plunger pump sliding shoe pair based on dynamic pressure effect. Hydraul Pneum 352(12):137–147
15. Tian Z-X (2018) Research on the supporting characteristics and influencing factors of hydrostatic thrust bearings. Huazhong University of Science and Technology
16. Fan J-W, Li X-Z, Mu D-H, Li W-H (2019) Optimization of key parameters of hydrostatic bearing based on CFX. Manuf Technol Mach Tool 07:37–43
17. Shao J, Xu L, Sun G (2020) Analysis of anti-eccentric load characteristics of hydraulic cylinder hydrostatic support. China Mech Eng 31(18):2174–2180
18. Pang Z (1981) Liquid gas static pressure technology. Heilongjiang People's Publishing House, Harbin
19. Chen Y, Sun G (1998) Principle and design of hydrostatic support. Beijing Aeronautical Institute Publishing
20. Ding Z (1986) Design of hydrostatic bearing. Shanghai Science and Technology Press
21. Stansfield FM (2003) Application of hydrostatic bearing in machine tools. China Machine Press, Beijing
22. Zhang BZ (2003) Numerical methods of fluid dynamics. China Machine Press, Beijing
23. ANSYS, Inc. (2007) ANSYS CFX-solver modeling guide. ANSYS, Inc.
24. Wang FJ (2004) Calculation flow mechanics analyses-FLUENT software principle and applies. TsingHua University Press, Beijing
25. Han Z, Wang J, Lan XP (2004) The FLUENT fluid project simulates calculating an example and applies. Press of Beijing Institute of Technology, Beijing
26. Wang Z (2018) Study on oil film stiffness performance ofhigh-speed and heavy load hydrodynamic and hydrostatic mixed lubrication thrust bearing. Harbin University of Science and Technology, Harbin